

DEVELOPMENT OF OFF-DESIGN TURBOCHARGER MODELLING COMBINED WITH 1-D ENGINE MODEL

A. Chun^a,
 C. C. M. Cunha^a,
 J. L. M. Donatelli^a,
 J. J. C. S. Santos^a,
 and C. B. Zabeu^b

^a Universidade Federal do Espírito Santo
 Departamento de Engenharia Mecânica
 Bairro Goiabeiras
 CP. 29075-910, Vitória, Espírito Santo, Brasil
 andr.chun@gmail.com
 carla@ele.ufes.br
 donatelliufes@gmail.com
 jjcssantos@yahoo.com.br

^bInstituto Mauá de Tecnologia
 Departamento de Engenharia Mecânica
 CP. 09580900, Mauá, São Paulo, Brasil.
 clayton@maua.br

Received: Dec 12, 2020
 Revised: Dec 29, 2020
 Accepted: Feb 01, 2021

ABSTRACT

The present work aims to carry out an off-design turbocharger modelling powered by exhaust gases from a Wärtsilä 20V34SG engine. First of all, 1-D engine model was already developed in GT-Power software while considering a thermodynamic turbocharger modelling with constant isentropic efficiencies. Secondly, by using the results from 1-D engine model, the off-design turbocharger modelling is calibrated separately in EES software, taking into account compressible assumption, triangle velocities and geometric dimensions. The case study is derived from a R&D project (ANEEL PD-06483-0318/2018) that targets to cool and dehumidify the intake air at compressor's upstream through a cooling coil, thereby allowing engine's operation at reduced knocking conditions. The brake mean effective pressure (BMEP) is varied in the range of 20 to 23.45 bar, corresponding to brake power from 8.7 to 10.2 MW, respectively. With the off-design turbocharger modelling it is possible to analyze its operational behavior under higher BMEP, hence, allowing to predict some important parameters. The results showed that the turbocharger is operating within the manufacturer's limit for BMEP of 23.45 bar, presenting total-to-static isentropic efficiencies of 0.81 and 0.784 for compressor and turbine, respectively, rotational speed around 28135 RPM, pressure ratio at compressor of 4.567 and maintaining control on waste-gate valve.

Keywords: turbocharger, off-design, internal combustion engine, thermodynamic, compressible

NOMENCLATURE

a speed of sound, m/s
 A area, m²
 c_p fluid specific heat at constant pressure, J/(kg.K)
 c_v fluid specific heat at constant volume, J/(kg.K)
 FP flow parameter
 h enthalpy, kJ/(kg K)
 k ratio of fluid specific heats
 ṁ mass flow rate, kg/s
 M mach number
 N rotation, RPM
 p fluid pressure, bar
 r radius, m
 RMS root mean square
 SR stage reaction
 T fluid temperature, K
 U rotational speed, m/s
 V fluid absolute velocity, m/s
 W fluid relative velocity, m/s

Greek symbols

α absolute flow angle, rad

β relative flow angle, rad
 Δ delta
 η efficiency
 π pressure ratio
 ρ density, kg/m³
 τ temperature ratio
 θ angular direction
 ω angular velocity, rad/s

Subscripts

a air
 dv diffuser vanes
 dyn dynamic
 g gases
 ib impeller blades
 j thermodynamic state
 in inlet
 out outlet
 nv nozzle vanes
 r radius direction
 rb rotor blades
 s isentropic
 ts total-to-static
 tt total-to-total

0 total property

Superscripts

c compressor
i type of component
t turbine

INTRODUCTION

Comprehending the physical phenomena that occur inside the turbocharger are challenging, in the literature there are several books with great amount of theoretical and practical information about the applications of turbochargers (Baskharone, 2006; Korpela, 2011; Turton, 2012). Regarding the maneuvers of turbocharger operation, there are several parameters that must be taken into account. Moreover, the turbocharger is quite sensible and maintaining always a safe operating condition can become a challenging task (McMillan, 2010). Usually, there are the compressor and turbine maps, which give enough information about the safest operating zones, allowing to operate without the occurrences of surge and choke conditions on air compressors and gas turbines (Dixon and Hall, 2013). Kurz *et al.* (2000) provide key information about how to build the gas turbine maps by using non-dimensional parameters such as Mach and Reynolds numbers, thermodynamic concepts, characteristics of each component and what parameters should be considered during the analysis.

Furthermore, most of the relevant works in this research field are developed on experimental bench scale tests and/or in extensive numerical simulations through commercial software. Regarding the practical situations, Brun and Nored (2006) presented a guideline for field testing of gas turbine and centrifugal compressor performance, providing a trade-off information about the performance degradation between field and factory tests, ensuring a proper validation of turbocharger functioning and a safe operating zone.

The surge effect on compressor was investigated by Freeman (2011) whose work treated compressor performance map generation and testing in line with SAE J1723. The author used a code written in Matlab software in order to plot the compressor map based on collected test data. Additionally, a comparison with test stand installation showed that his technique was more accurate with less time consuming on performing the process. With respect to rotating stall, Bently *et al.* (2001) investigated through experiments this phenomenon in centrifugal compressors from the standpoint of rotor dynamics. According to the authors, the most significant conclusion was related to aerodynamic forces applied to the impeller which generated negative radial stiffness. In addition, the stiffness dropped even more during the rotating stall.

Another work from Gravidahl (1998) modelled and simulated the control of surge and rotating stall in compressors by using Moore-Greitzer compression system which takes into account disturbances, constant and time varying. In summary, it is not an easy or simple task to model and simulate these physical phenomena that occur inside the turbomachinery, thereby, requiring more complex relations and mathematical tools to solve the problem.

There are several works in the literature exploring distinct strategies to model, design and predict turbomachinery behavior through numerical simulations and testing experiments. For example, Liedman and Månsson (2013) simulated dynamically a centrifugal compressor system in HYSYS Dynamics™ software, validating the simulations with operating data from the site. A designing project of centrifugal compressor was developed by Campos (2013) for small gas turbine applications, his methodology consisted on using non-dimensional variables with thermodynamic and compressible analyses, also numerical simulations in CFD were utilized to define the compressor 3D geometry. Duda (2017) studied the turbocharger compressor performance by operating with an alternative gas. He carried out experimental tests and some CFD simulations, investigating the performance and surge effects. In short, a comparison between the experimental and numerical results of the compressor performance showed that for homogeneously and non-homogeneously substitute gas presented none considerable changes on compressor performance.

When turbochargers and intercooling process are combined with internal combustion engines, the goal is to fill great amount of air into piston-cylinders, thereby, enhancing the combustion process, and consequently, producing more brake shaft power output (Watson and Janota, 1982; Taylor, 1985; Bell, 1997). Mamat *et al.* (2012) simulated in commercial CFD software and validated through test rig the development of a low-pressure turbine for turbocharger application in a gasoline engine which was also developed in 1-D engine model with three catalytic arrangements. In their results, it was reached a maximum benefit of the turbocharger application at post catalytic position, reducing the BSFC around 2.4% with 1,500 RPM and increasing 3.0% of BMEP with 1,000 RPM.

Regarding the compressor map, Sorenson *et al.* (2005) developed an accurate modelling for any radial compressor through some dimensionless correlations, allowing to analyse the performance either for spark or diesel engines. However, his methodology required to test six different compressors in order to define the necessary constants. Another work from Serrano *et al.* (2008) developed a model of fixed and variable geometry for turbine equipment, permitting to define some efficient boundary conditions to model turbocharged

internal combustion engines with one dimensional gas dynamic codes.

The purpose of this paper is to fill the gap in regard to none available analytic method on evaluating an off-design modelling of turbocharger equipment coupled with W20V34SG engine. A method based on analytic approach utilizing compressible relations, triangle velocities technique and geometric dimensions is proposed as an alternative way to deal with the physical phenomena inside the turbocharger. In order to accomplish this objective, some data from 1-D engine model in GT-Power simulations are used as parameters and new simulations of turbocharger modelling in EES software are carried out, therefore, comparing the final results with the turbocharger modelling of GT-Power simulations which was assumed as a thermodynamic modelling with constant isentropic efficiencies (Zabeu *et al.*, 2008).

CASE STUDY

The case study is derived from a R&D project (ANEEL PD-06483-0318/2018) at Luiz Oscar Rodrigues de Melo thermal power plant (UTE LORM) which accounts with twenty-four Wärtsilä 20V34SG engines of 8.7 MW that are fueled with natural gas from PETROBRAS facilities. All of them count on 2 NAPIER 307 turbochargers with maximum rotation speed of 29500 RPM and maximum pressure ratio of 5:1 (Napier, 2017). The turbocharger is composed by a single stage radial compressor and single stage axial turbine. At the mentioned application, the radial compressors deliver air to the engine's charge air cooler (CAC) at approximated 3.8 bar of absolute pressure and 473 K of total temperature under an engine's brake power output of 8.7 MW, i.e., BMEP equal 20 bar. As compressor and turbine maps are key elements of turbocharger performance, manufactures do not make them available for end users. Hence, if one intends to study the other operational conditions of engine and turbochargers while exploring the potential gains under an inlet air lower temperature and humidity, it is necessary to develop and calibrate models to predict the overall behavior of the turbocharger.

Figure 1 (a) represents the radial compressor and axial turbine similar to ones present in Napier 307 turbocharger. Moreover, the radial compressor is a backward curved configuration while axial turbine is a single stage structure. Each thermodynamic state is calculated in this turbocharger.

The geometric characteristics are defined in Table 1, notwithstanding it is relevant to note that some information are approximated by analysing some available technical drawings. The subscript *i* refers to the compressor or turbine component.

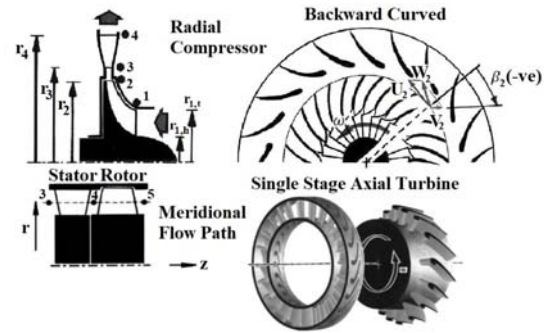


Figure 1. Schematic of compressor and turbine geometries. Source: Adapted from Baskharone (2006).

Table 1. Turbocharger geometric characteristics.

Parameter	Radial compressor	Axial Turbine
n_{dv} and n_{nv}	16 vanes	24 vanes
n_{ib} and n_{tb}	18 blades	53 blades
$r_{1/3,tip}^t$	0.11 m	0.26 m
$r_{1/3,hub}^t$	0.04 m	0.20 m
r_2^c	0.16 m	-
r_3^c	0.18 m	-
r_4^c	0.25 m	-
e_{rotor}^t	-	0.003 m
$e_{in,nv}^t$	-	0.013 m
$e_{out,nv}^t$	-	0.001 m

METHODOLOGY

In this section, it is presented an analytic approach to model the turbocharger by assuming compressible effects, triangle velocities technique and geometric data. This methodology is based on well-established principles of turbomachinery technology from the literature (Baskharone, 2006; Dixon and Hall, 2013; Korpela, 2011; Turton, 2012).

A list of assumptions is also necessary to simplify this modelling; (i) steady state, (ii) adiabatic condition, (iii) specific heats and coefficient *k* are constant, (iv) potential energy is neglected, (v) ideal gases behavior, (vi) free vortex in radial direction inside the compressor, and (vii) compressible effects are accounted in the modelling, as well as, triangle velocities and the geometric aspects.

In agreement with the literature, the governing equations of compressible phenomena are presented below in function of Mach number (M_j), total and static thermodynamic properties such as temperatures, pressures and densities ($T_{j,0}$, $p_{j,0}$, $\rho_{j,0}$, $T_{j,0}$, p_j and ρ_j), speed of sound (a_j), and fluid properties (k_j , \bar{R}_j and \bar{M}_j). Subscripts 0 refers to total property while subscript *j* assigns each thermodynamic state. Equation 1 to Equation 6 present the fundamental governing equations of compressible phenomena.

$$\frac{T_{j,0}}{T_j} = 1 + \frac{(k_j - 1) \cdot M_j^2}{2} \quad (1)$$

$$\frac{p_{j,0}}{p_j} = \left[1 + \frac{(k_j - 1) \cdot M_j^2}{2} \right]^{\frac{k_j}{k_j - 1}} \quad (2)$$

$$\frac{\rho_{j,0}}{\rho_j} = \left[1 + \frac{(k_j - 1) \cdot M_j^2}{2} \right]^{\frac{1}{k_j - 1}} \quad (3)$$

$$a_j = \sqrt{k_j \cdot R_j \cdot T_j} \quad (4)$$

$$M_j = \frac{V_j}{a_j} \quad (5)$$

$$R_j = \frac{\bar{R}_j}{M_j} \quad (6)$$

The ratio k for air is adopted around 1.4, while for exhaust gases, the coefficient k must be calculated assuming an average between inlet and outlet k 's of thermodynamic states in the turbine, as it is presented in Eq. 7. Thus, Eq. 8 calculates each k by dividing the specific heats, $c_{p,j}$ over $c_{v,j}$. In this case, k_g^t is equal to 1.35 while $c_{p,j}$ is 1.132 kJ/(kg K).

$$k_g^t = \frac{k_{in}^t + k_{out}^t}{2} \quad (7)$$

$$k_j^t = \frac{c_{p,j}}{c_{v,j}} \quad (8)$$

The triangle velocities technique is necessary because kinetic energy is not neglected in this modelling. And an essential parameter known as stage reaction (SR_i) must be analysed for each component. These stages reactions are computed by acknowledging the enthalpy variations (Δh_j^i) which are in function of rotational speed (U_j^i), absolute (V_j^i) and relative velocities (W_j^i). For radial compressor, Eq. 9 to Eq. 11 estimate the stage reaction in this component.

$$\Delta h_{static}^c = \frac{(\bar{W}_1^c)^2 - (W_2^c)^2 + (U_2^c)^2 - (\bar{U}_1^c)^2}{2} \quad (9)$$

$$\Delta h_{dyn}^c = \frac{(V_2^c)^2 - (V_1^c)^2}{2} \quad (10)$$

$$\Delta h_{total}^c = \Delta h_{static}^c + \Delta h_{dyn}^c \quad (11)$$

The stage reaction in the turbine is calculated by Eq. 12 and Eq. 13.

$$\Delta h_{static}^t = \frac{(W_5^t)^2 - (W_4^t)^2}{2} \quad (12)$$

$$\Delta h_{total}^t = \frac{(W_5^t)^2 - (W_4^t)^2 + (V_4^t)^2 - (V_5^t)^2}{2} \quad (13)$$

Hence, in Fig. 2, it is presented the triangle velocities for radial compressor and axial turbine, respectively.

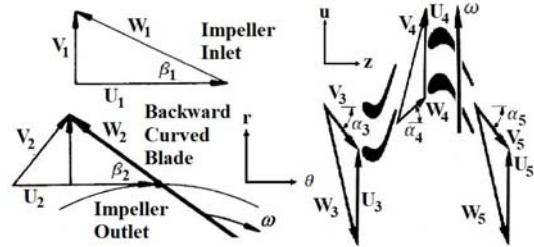


Figure 2. Radial compressor (a) and axial turbine (b) triangle velocities. Source: Adapted from Turton (2012) and Baskharone (2006).

The following vectorial Eq. 14 is applied for each triangle velocity. Further, the absolute flow angle on the compressor's inlet (α_1^c) is null, i.e. it means that air stream is flowing perpendicularly to the impeller. For turbine, the inlet and outlet absolute flow angles (α_3^t and α_5^t) are assumed as null values too.

$$V_j^i = W_j^i + U_j^i \quad (14)$$

The rotational speed can be evaluated by Eq. 15 and Eq. 16.

$$U_j^i = \omega_i \cdot \bar{r}_j^i \quad (15)$$

$$\omega_i = \frac{2 \cdot \pi \cdot N_i}{60} \quad (16)$$

Regarding the radial compressor, each velocity in r -direction and θ -direction are represented by Eq. 17 to Eq. 20.

$$V_{j,\theta}^c = V_j^c \cdot \cos \alpha_j^c \quad (17)$$

$$V_{j,r}^c = V_j^c \cdot \sin \alpha_j^c \quad (18)$$

$$W_{j,\theta}^c = W_j^c \cdot \cos \beta_j^c \quad (19)$$

$$W_{j,r}^c = W_j^c \cdot \sin \beta_j^c \quad (20)$$

The same equations are repeated for turbine triangle velocities but in z -direction and u -direction, as explicit in Eq. 21 to Eq. 24.

$$V_{j,z}^t = V_j^t \cdot \cos \alpha_j^t \quad (21)$$

$$V_{j,u}^t = V_j^t \cdot \sin \alpha_j^t \quad (22)$$

$$W_{j,z}^t = W_j^t \cdot \cos \beta_j^t \quad (23)$$

$$W_{j,u}^t = W_j^t \cdot \sin \beta_j^t \quad (24)$$

When evaluating the turbine, it is necessary to define the flow parameter ($FP_{j,0}^t$) which is represented by Eq. 25 and Eq. 26. Both equations relate thermodynamic and kinetic properties with geometric aspects.

$$FP_{j,0}^t = \frac{\dot{m} \cdot \sqrt{T_{j,0}^t} \cdot \frac{R_g}{k_g}}{p_{j,0}^t \cdot A_j^t \cdot \cos(\alpha_j^t)} \quad (25)$$

$$FP_{j,0}^t = M_{j,t} \cdot \left(1 + \frac{k_g - 1}{2} \cdot M_{j,t}^2 \right)^{\frac{(k_g + 1)}{2(1 - k_g)}} \quad (26)$$

Table 2 summarizes separately other fundamental equations for each component in the turbocharger.

Table 2. Fundamental equations for air compressor and gas turbine.

Parameter	Radial Compressor	Axial Turbine
η_{is}^i	$\frac{\left(\frac{p_{out}^c}{p_{in,0}^c}\right)^{\frac{k_a-1}{k_a}} - 1}{\tau_c - 1}$	$\frac{1 - \tau_t}{1 - \left(\frac{p_{out}^t}{p_{in,0}^t}\right)^{\frac{k_g-1}{k_g}}}$
η_{it}^i	$\frac{\pi_c^{\frac{k_a-1}{k_a}} - 1}{\tau_c - 1}$	$\frac{1 - \tau_t}{1 - \pi_t^{\frac{k_g-1}{k_g}}}$
SR_i	$\frac{\Delta h_{static}^c}{\Delta h_{total}^c}$	$\frac{\Delta h_{static}^t}{\Delta h_{total}^t}$
\dot{m}_j^i	$\rho_a \cdot V_j^c \cdot A_j^c$	$\rho_g \cdot V_j^t \cdot A_j^t$
π_i	$\frac{p_{out,0}^c}{p_{in,0}^c}$	$\frac{p_{in,0}^t}{p_{out,0}^t}$
τ_i	$\frac{T_{out,0}^c}{T_{in,0}^c}$	$\frac{T_{in,0}^t}{T_{out,0}^t}$

After defining the governing equations as well as other auxiliary equations to correlate kinetic energy with thermodynamic properties and geometric characteristics, it is important to discuss the first calibration in this modelling.

When dealing with radial compressor, in this case, backward configuration, the relative angle β_2 must be set for calculation purposes. However, as this information is not given even from manufacturer, the first calibration is executed by using some operating data from the site in order to determine β_2 .

Regarding the operating condition, this radial compressor shall not present supersonic flow inside the compressor. As it has a diffuser just after the impeller, if the incoming flow stream achieves supersonic speed, this device will work as a supersonic nozzle, increasing the velocity while decreasing the pressure. Thereupon, in an effort to avoid this situation, the Mach number at impeller's exit must be lesser than unit, i.e. the diffuser will work in subsonic flow, which implicates in increasing the pressure while decreasing the velocity.

In Figure 3, the pressure ratio, total temperature and Mach number at impeller's exit are plotted in function of relative angle β_2 . The chart of pressure ratio in function of β_2 allows to determine this relative angle in Fig. 3 (a), then, by considering a pressure ratio of 3.8 bar, β_2 is defined as -45° which is inside the backward curved region. Furthermore, the total temperature at compressor exit is usually around 200°C (473.15 K), thereby, respecting the manufacturer's recommendation. By analysing Fig. 3 (b), it is checked that the Mach number at diffuser is not in supersonic flow. Therefore, this first calibration respects all operating conditions in this radial compressor. In order to generate these charts in function of relative angle β_2 , it is adopted impeller's efficiency around 0.8192, and rotational speed of 26,150 RPM with an air mass flow rate of 6.7 kg/s in one radial compressor. These previous values are based on UTE LORM database and some information from the literature.

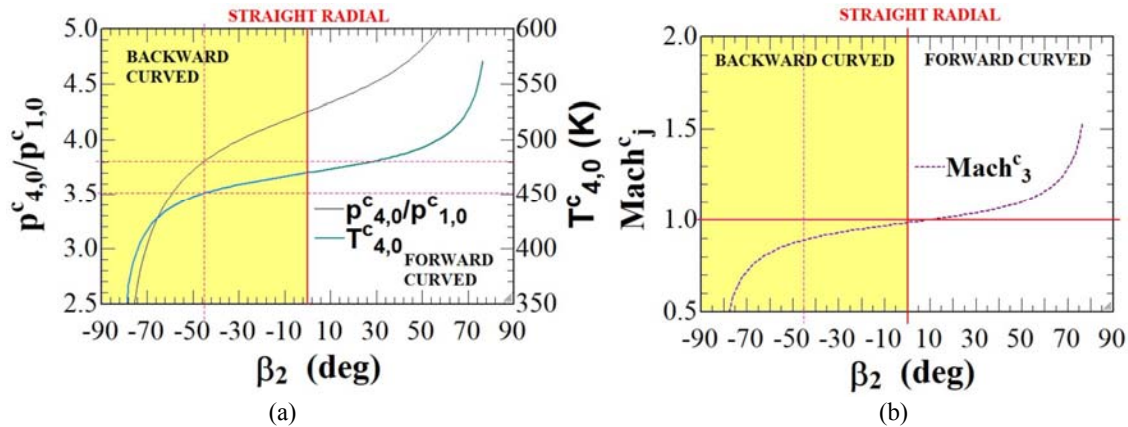


Figure 3. Calibrating relative angle by matching with operating pressure ratio (3.8 bar) (a) and at diffuser's inlet by verifying the flow condition at radial compressor (b).

A first turbocharger modelling was carried out in GT-Power software by assuming constant isentropic efficiencies for both compressor and turbine. Then, as the 1-D engine is simulated by varying BMEP in a range of 20 to 23.45 bar, there are some results from this first turbocharger modelling that are used as curve fitting equations.

The induced pressure drop (Δp_{in}^c) caused by the cooling coil at compressor's upstream is considered in the modelling and as the ambient pressure is 1.01325 bar, the inlet total pressure at radial compressor ($p_{1,0}^c$) can be calculated by subtracting the induced pressure drop from ambient pressure.

The static temperature at the entry of radial compressor ($T_{1,0}^c$) is also extracted from GT-Power

simulations. Moreover, the cooling coil delivers a total temperature ($T_{1,0}^c$) of 285.65 K.

The total pressure at compressor's exit ($p_{4,0}^c$) is also considered as an input parameter, as well as, the air mass flow rate (\dot{m}_a) on radial compressor.

The inlet ($p_{3,0}^t$ and $T_{3,0}^t$) and outlet total properties ($p_{5,0}^t$) at turbine component are needed as input parameters too. Table 3 summarizes the curve fitting equations from the GT-Power simulations with the corresponding root mean square values (RMS) and physical units. The R^2 for each curve fitting equation is 100%.

Table 3. Curve fitting equations from GT-Power simulations for BMEP in a range of 20 to 23.45 bar.

Parameter	Curve Fitting Equations	RMS	Unit
Δp_{in}^c	$\frac{-240,494+49,880.3 \cdot \text{BMEP}+47,448 \cdot \text{BMEP}^2+65.5325 \cdot \text{BMEP}^3}{10^8}$	$2.5 \cdot 10^{-13}$	bar
$T_{1,0}^c$	$\frac{286,388-67.6281 \cdot \text{BMEP}+0.682831 \cdot \text{BMEP}^2-0.0493137 \cdot \text{BMEP}^3}{10^3}$	$4.1 \cdot 10^{-12}$	K
$P_{4,0}^c$	$\frac{325,948+164,976 \cdot \text{BMEP}+415.884 \cdot \text{BMEP}^2+9.49015 \cdot \text{BMEP}^3}{10^6}$	$1.2 \cdot 10^{-12}$	bar
\dot{m}_a	$\frac{762,937+665,159 \cdot \text{BMEP}+975.639 \cdot \text{BMEP}^2+25.6431 \cdot \text{BMEP}^3}{2 \cdot 10^6}$	$3.1 \cdot 10^{-15}$	kg/s
$P_{3,0}^t$	$\frac{481,669+97,586.4 \cdot \text{BMEP}+1,434.14 \cdot \text{BMEP}^2+1.17257 \cdot \text{BMEP}^3}{10^3}$	$5.7 \cdot 10^{-12}$	bar
$T_{3,0}^t$	$\frac{731,442+2,516.12 \cdot \text{BMEP}-32.5323 \cdot \text{BMEP}^2+0.20383 \cdot \text{BMEP}^3}{10^3}$	$5.7 \cdot 10^{-12}$	K
$P_{5,0}^t$	$\frac{994,344+1,436.76 \cdot \text{BMEP}+37.2434 \cdot \text{BMEP}^2-0.142462 \cdot \text{BMEP}^3}{10^6}$	$2.2 \cdot 10^{-12}$	bar

Therefore, another important goal is to analyse if the total-to-static isentropic efficiencies in this off-design modelling are going to change abruptly or not. Further, it is possible to predict with this methodology the amount of shaft work in the turbocharger as well as the rotational speed.

The air-fuel ratio (A/F) is a dimensionless value of 34.53, maintaining excess of air around 2. As the air mass flow rate and air-fuel ratio are set as parameters, the amount of fuel (\dot{m}_f) is easily calculated by applying Eq. 27.

$$A/F = \frac{\dot{m}_a}{\dot{m}_f} \quad (27)$$

The exhaust gases mass flow rate (\dot{m}_g) is sequentially determined by using Eq. 28. At last, it is possible to estimate the amount of gases passing through the waste-gate valve (\dot{m}_{wg}) by applying mass and energy balance, as represented in Eq. 29 and Eq. 30, respectively.

$$\dot{m}_g = \dot{m}_a + \dot{m}_f \quad (28)$$

$$\dot{m}_g = \dot{m}_t + \dot{m}_{wg} \quad (29)$$

$$\dot{m}_a \cdot (h_{4,0}^c - h_{1,0}^c) = \dot{m}_t \cdot (h_{3,0}^t - h_{5,0}^t) \quad (30)$$

As there are other parameters that must be set during the simulations in EES software, a second calibration is carried out by targeting simultaneously the total temperature at the exit of radial compressor of 452.8 K, waste-gate mass flow rate of 0.3908 kg/s, and total-to-static efficiencies of 0.8 at compressor and turbine components. The compressor impeller's efficiency (η_{imp}) as well as turbine's polytropic efficiency (η_p), tip and hub radius are slightly corrected to match the values from GT-Power simulations considering BMEP of 20 bar.

RESULTS AND DISCUSSION

The first result regards to compare the waste-gate mass flow rates between this off-design methodology and the GT-Power simulations, as presented in Fig. 4 (a). When assuming compressible effects and using more complex relations to determine the turbocharger operating behavior, it is

observed that waste-gate mass flow rate is higher than the GT-Power result, which considered the turbocharger with constant isentropic efficiencies for both compressor and turbine. As the waste-gate valve is more open, the turbine mass flow rates in this proposed modelling are smaller than turbine mass flow rates from GT-Power, as explicit in Fig. 4 (b). The graphs are accounting two turbocharger per engine.

These differences can be explained due an increasing in stage reaction in turbine which is presented in Fig. 5 (a). The reaction is rising slightly when BMEP is increasing, which means that less exhaust gases are necessary in the turbine. Another advantage on using these detailed equations from this proposed methodology is regarded to estimate the operating speed and turbocharger shaft work for each BMEP. In Fig. 5 (b), it is shown both of these results.

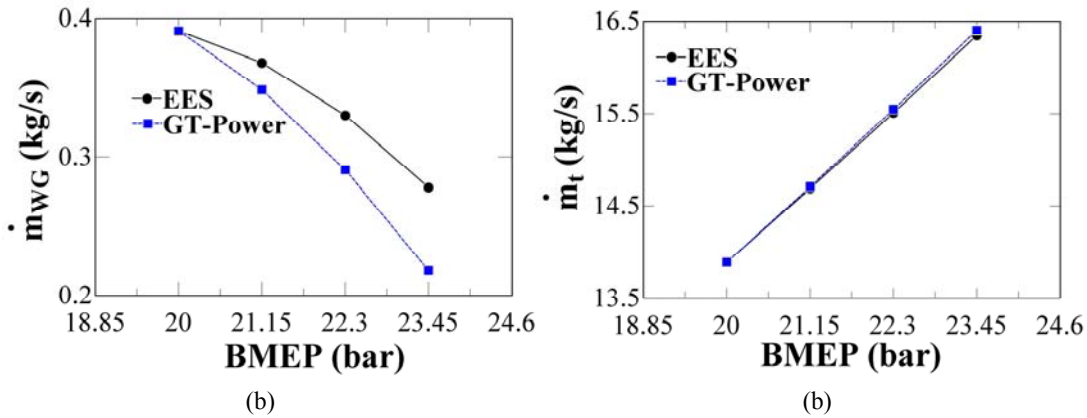


Figure 4. Comparison of waste-gate (a) and turbine mass flow rates (b) in function of BMEP.

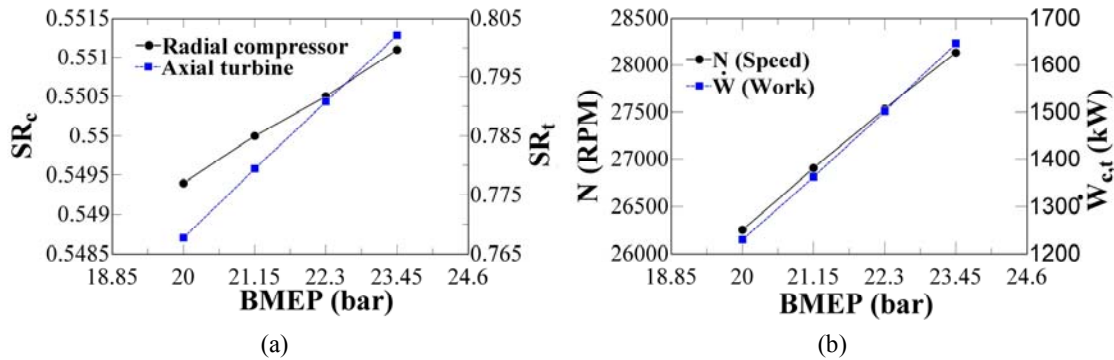


Figure 5. Stage reaction profiles (a), rotational speed and shaft work (b) in function of BMEP.

The total-to-static efficiencies are calculated at each BMEP for both compressor and turbine. It is essential to state that these efficiencies are not constant at all. Nevertheless, by analysing Fig. 6 (a), there are small changes in these efficiencies. It is interesting to note that the turbine's total-to-static efficiency is more sensible than compressor's efficiency in function of BMEP. Moreover, the turbine's efficiency decreases while compressor's efficiency rises for each BMEP.

Despite the fact that the operating characteristics are affected directly by the isentropic efficiencies, the results of this off-design modelling

show small changes in the total-to-static isentropic efficiencies at each BMEP. The temperature at compressor's exit is following GT-Power result with a small difference, which makes sense since it was used same parameters in this modelling and compressor's efficiency did not change abruptly. In Fig. 6 (b), the outlet temperature at turbine component from this methodology is lower than GT-Power result. This behavior makes sense since turbine is gaining stage reaction, and less mass flow rate is entering in the turbine. Hence, the enthalpy difference in the turbine increases to keep the same amount of shaft work.

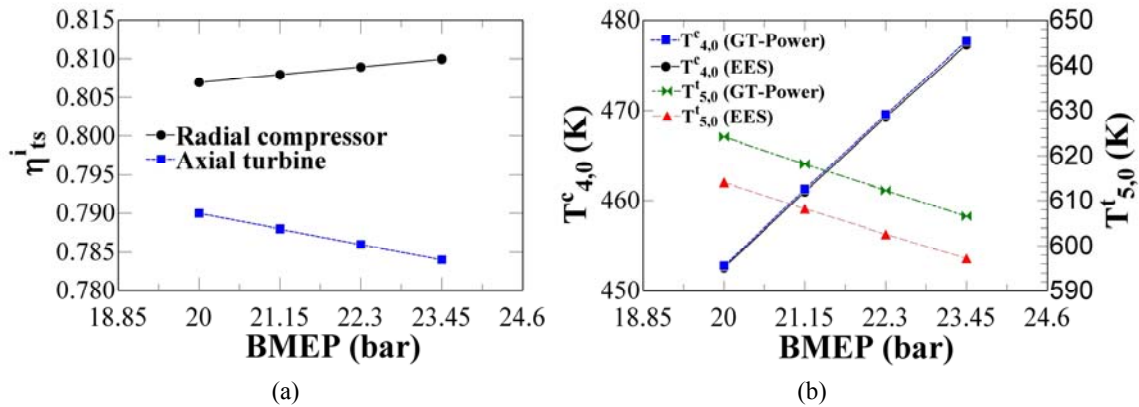


Figure 6. Total-to-static efficiencies (a) and total temperatures (b) in function of BMEP.

CONCLUSIONS

This methodology has been developed in order to approach analytically the NAPIER 307 turbocharger by assuming compressible effects with triangle velocities and geometric data. A first turbocharger modelling using constant isentropic efficiencies was developed in GT-Power software, thereby, in an effort to verify whether the results of this paper are demonstrating a coherent behavior, the waste-gate and turbine mass flow rates, and temperatures of exhaust gases are compared to GT-Power results.

Indeed, this off-design modelling has a lot of simplifications and basic assumptions that interfere significantly in the final results. As this present paper has a methodology based on geometric dimensions of a specific turbocharger from Napier's manufacturer, it is quite difficult to find in the literature or technical reports similar results with the same NA307 turbocharger. This off-design turbocharger modelling is not free of errors, for future works, the results of this paper should be validated with experimental tests at UTE LORM by comparing with operating data.

The main results are related to the advantage on predicting the speed and total-to-static isentropic efficiencies of the single-stage radial compressor and single-stage axial turbine. As it is targeted to increase the BMEP to 23.45 bar, the off-design turbocharger modelling provides results that are within in the manufacturer's recommendations, presenting rotational speed of 28135 RPM, pressure ratio at compressor component around 4.567, total-to-static isentropic efficiencies of 0.81 and 0.784 for compressor and turbine, respectively. Furthermore, the waste-gate valve opening is still under control, presenting a mass flow rate of 0.278 kg s⁻¹. Therefore, for the purpose of the R&D project, the NA307 turbocharger will probably operate under acceptable conditions.

ACKNOWLEDGEMENTS

The authors are thankful to the Program of Research and Development of the Electric Energy Sector regulated by the Brazilian Electricity Regulatory Agency - ANEEL, Coordination for the Improvement of Higher Education Personnel - CAPES and Viana S.A. Thermoelectric Power Plant - TEVISA, an electric power generating company that provided financial support for this project.

REFERENCES

- Baskharone, E. A., 2006, Principles of turbomachinery in air-breathing engines, Cambridge University Press.
- Bell, C., 1997, Maximum boost: designing, testing, and installing turbocharger systems, Robert Bentley Automotive Publishers.
- Bently, R., Goldman, P. and Yuan, J., 2001, "Rotor dynamics of centrifugal compressors in rotating stall", Bentley Rotor Dynamics Research Corporation, Tech. Rep.
- Brun, K. and Nored, M., 2006, "Guideline for field testing of gas turbine and centrifugal compressor performance".
- Report, August. Campos, A. P. V. D., 2013, Desenvolvimento de um compressor radial para turbina a gás de pequeno porte, Doctoral Thesis, Universidade de São Paulo, São Paulo, SP.
- Dixon, S. L. and Hall, C., 2013, Fluid mechanics and thermodynamics of turbomachinery, Butterworth-Heinemann.
- Duda, T., 2017, Turbocharger performance and surge definition on a steady flow turbocharger test stand. Doctoral thesis, University of Bath, Bath, Som.
- Freeman, J. L., 2011, "Compressor performance map generation and testing per sae j1723".
- Gravdahl, J. T., 1998, "Modeling and control of surge and rotating stall in compressors", Doctoral Thesis, Department of Engineering Cybernetics.
- Korpela, S. A., 2011. Principles of turbomachinery. Wiley Online Library, New Jersey.

Kurz, R., Brun, K., 2000, "Gas turbine performance-what makes the map?", in: Proceedings of the 29th Turbomachinery Symposium, Texas A&M University, Turbomachinery Laboratories.

Liedman, J. and Månsson, R., 2013, Dynamic simulation of a centrifugal compressor system, Master's Thesis, Chalmers University of Technology, Gothenburg.

Mamat, A. M., Romagnoli, A. and Martinez-Botas, R. F., 2012, "Design and development of a low-pressure turbine for turbocompounding applications", *International Journal of Gas Turbine, Propulsion and Power Systems*, Vol. 4, No. 3, pp. 1–8.

McMillan, G. K., 2010, *Centrifugal and axial compressor control*, Momentum Press, North Carolina.

Napier, 2017, "Na 307 operator's manual". Technical report, Wärtsilä, URL www.napier-turbochargers.com.

Serrano, J., Arnau, F., Dolz, V., Tiseira, A. and Cervelló, C., 2008, "A model of turbocharger radial turbines appropriate to be used in zero- and one-dimensional gas dynamics codes for internal combustion engines modelling", *Energy Conversion and Management*, pp. 3729–3745.

Sorenson, S. C., Hendricks, E., Magnusson, S. and Bertelsen, A., 2005, "Compact and accurate turbocharger modelling for engine control", *SAE transactions*, pp. 1343–1353.

Taylor, C. F., 1985, *The Internal-combustion Engine in Theory and Practice: Combustion, fuels, materials, design*, Vol. 2. MIT press.

Turton, R. K., 2012, *Principles of turbomachinery*, Springer Science & Business Media, New Jersey.

Watson, N. and Janota, M., 1982, *Turbocharging the internal combustion engine*, Macmillan International Higher Education.

Zabeu, C., Martelli, A. and Penaranda, A., 2008, "Projeto de p&d - diagnóstico de problemas, otimização da combustão e balanceamento da potência de cilindros de motores a gás natural". Technical report, Wärtsilä.